PHOTONICS Research

Nonlinear Fourier transform enabled eigenvalue spectrum investigation for fiber laser radiation

Yutian Wang,[1] Songnian Fu,[2] Jian Kong,[3] Andrey Komarov,[4] Mariusz Klimczak,[5] Ryszard Buczyński,[5] Xiahui Tang,[1] Ming Tang,[1] Yuwen Qin,[2] and Luming Zhao[1,*]

[1]School of Optical and Electronic Information and Wuhan National Laboratory for Optoelectronics, Huazhong University of Science and Technology, Wuhan 430074, China
[2]Advanced Institute of Photonics Technology, School of Information Engineering, and Guangdong Provincial Key Laboratory of Information Photonics Technology, Guangdong University of Technology, Guangzhou 510006, China
[3]Kunshan Shunke Laser Technology Co., Ltd., Suzhou 215347, China
[4]Institute of Automation and Electrometry, Russian Academy of Sciences, Novosibirsk 630090, Russia
[5]Faculty of Physics, University of Warsaw, Warsaw 02-093, Poland
*Corresponding author: lmzhao@ieee.org

Received 19 April 2021; revised 8 June 2021; accepted 9 June 2021; posted 11 June 2021 (Doc. ID 427842); published 29 July 2021

Fiber lasers are a paradigm of dissipative systems, which distinguish themselves from a Hamilton system where energy is conservative. Consequently, pulses generated in a fiber laser are always accompanied by the continuous wave (CW). Under certain hypothesis, pulses generated in a fiber laser can be considered as a soliton, a product of a Hamilton system. Therefore, all the descriptions of solitons of a fiber laser are approximate. Coexistence of solitons and the CW from a fiber laser prevents unveiling of real nonlinear dynamics in fiber lasers, such as soliton interactions. Pulse behavior in a fiber laser can be represented by the state of single pulse, the state of period doubling of single pulse, the states of two pulses either tightly bound or loosely distributed, the states of three pulses, and various combinations of the above-mentioned states. Recently, soliton distillation was proposed and numerically demonstrated based on the nonlinear Fourier transform (NFT) [J. Lightwave Technol. 39, 2542 (2021)]. Solitons can be separated from the coherent CW background. Therefore, it is feasible to isolate solitons from CW background in a fiber laser. Here, we applied the NFT to various pulses generated in a fiber laser, including single pulse, single pulse in period doubling, different double pulses, and multiple pulses. Furthermore, with the approach of soliton distillation, the corresponding pure solitons of those pulses are reconstructed. Simulation results suggest that the NFT can be used to identify soliton dynamics excluding CW influence in a fiber laser, which paves a new way for uncovering real soliton interaction in nonlinear systems.

https://doi.org/10.1364/PRJ.427842

1. INTRODUCTION

In steady-state operation, mode-locked lasers can generate highly stable pulse trains, which have various applications in science and engineering [1,2]. From the applications perspective, the ultrafast fiber laser offers its inherent advantages of robust operation and compact footprint [3,4]. Beyond its very evident practical importance, ultrafast fiber lasers are also interesting from the standpoint of physics as a platform for investigating various aspects of nonlinear wave dynamics [5–7]. Getting a considerable insight into the nonlinear dynamics and instabilities of fiber lasers is promising for discovering new operation regimes with potentially superior characteristics [8]. In contrast to a light pulse propagation over a fiber—where the system is conservative with the assumption of lossless propagation—a fiber laser is a paradigm of dissipative systems, where gain and loss affect the pulse generation, while simultaneously it is a periodic boundary system. Due to these dynamical changes, nonstationary pulses cannot be efficiently represented by the use of a linear combination of stationary signals. Therefore, traditional Fourier transform is not always suitable for investigation of fiber laser radiation. To solve this technological hurdle, several advanced characterization methodologies have been demonstrated, providing new ultrafast measurement tools to reveal transient phenomena arising in nonlinear laser dynamics. For instance, the dispersive Fourier transform (DFT) method has been successfully applied in fiber lasers for investigating soliton explosions [9], bound solitons [10,11], transition dynamics from Q-switching to mode locking [12], and buildup dynamics of harmonic mode locking [13]. Furthermore, the methodology of space–time duality has been successfully exploited to realize time lenses for direct

observation of rogue waves [14] and unknown soliton dynamics [15]. It is now well known that, when solitons are generated in fiber lasers, there appear sidebands on the spectrum, such as Kelly sidebands [16] and other incoherent sidebands [17]. The incoherent sidebands can be removed by reducing pump power or intracavity polarization modulation, while the coherent sidebands such as Kelly sidebands always exist. Kelly sidebands could be considered as one of the resonant continuous wave (CW) backgrounds [18]. Although the DFT and time lens methods have successfully realized laser output monitoring in real time, the dynamics of solitons alone or of a pure soliton in a cavity is still unclear.

Recently, an elegant method of nonlinear Fourier transform (NFT) has attained attraction in the ultrafast optics community [19]. It is a powerful mathematical tool, which enables solving problems of wave propagation in some nonlinear media, especially in the field of soliton theory. Also known as inverse scattering transform, the NFT can decompose the signal into a continuous spectrum (nonsoliton components) and a discrete spectrum (soliton components) to obtain the corresponding nonlinear spectrum [20]. With the help of such an approach, information can be encoded into the nonlinear spectrum of the signal, which can effectively address the nonlinear transmission impairments arising in standard single-mode fiber (SMF) transmission [21,22]. Meanwhile, as a method to obtain analytic solutions to the nonlinear Schrödinger equation (NLSE), the NFT can be used to analyze signals in optical fibers, such as rogue waves [23] and Kerr optical frequency combs [24]. In particular, such NFT methodology provides a viewpoint on the new physics of laser dynamics. Specifically, the NFT has been shown to have the capability to characterize the ultrashort pulse in the nonlinear frequency domain [25–27]. Based on the NFT, we have proposed a method of soliton distillation to distinguish solitons from the resonant CW background according to their different eigenvalue distributions [28].

Fiber lasers operated in steady states can be classified into the state of single pulse, the state of period doubling of single pulse, the states of dual pulses either tightly bound or loosely distributed, the states of three pulses, and various combinations of the above-mentioned states. Since fiber lasers are a paradigm of dissipative systems, all the pulses sustained with the CW background. It is interesting to understand the performance of soliton alone in a fiber laser. As the CW always functions as an energy buffer, it is fundamental to get insight into soliton interaction without the CW. Therefore, we can use the approach of NFT-based soliton distillation to separate solitons from the CW background. We noted that we applied the NFT to deal with signal output from the fiber laser, not the one inside the fiber laser cavity.

In the following section, we report on the dynamics of various stable states arising in a fiber laser after the NFT is applied, including the state of single pulse, the state of single pulse in period doubling, and the states of double pulses and triple pulses. Furthermore, by using the approach of soliton distillation, we recover the pure solitons of those pulses. It is verified that the CW background indeed buffers solitons and affects the performance of coexisting solitons. The results provide a unique insight of the internal evolution of pure solitons without the CW background influence.

2. RESULTS AND DISCUSSIONS

The details of NFT processing can be found in Appendix A. A typical output of the passively mode-locked fiber laser and its optical spectrum are shown in Figs. 1(a) and 1(b). Different from theoretical soliton, there is a pedestal arising in the temporal profile and Kelly sidebands symmetrically exist in its optical spectrum. The eigenvalues distribution is shown in Fig. 1(c). The eigenvalue corresponding to the soliton has large imaginary parts and almost zero real parts, which indicates that the soliton has a near-zero velocity. The imaginary part of the soliton eigenvalue is only determined by the amplitude of the pulse. Meanwhile, distinctly from the eigenvalue distribution of a theoretical soliton, some eigenvalues have nonzero real parts and relatively small imaginary parts, indicative of nonzero velocities of the corresponding temporal features of the resonant CW background. The real parts of CW eigenvalues are related to its frequency.

Obviously, the eigenvalues of the pulse from the fiber laser are different from that of a theoretical soliton, which is attributed to the coexisting resonant CW background. Since the soliton and the resonant CW background have different eigenvalue distributions, it is feasible to separate a pure soliton from the resonant CW background based on the NFT. Then, we select the eigenvalue corresponding to the soliton and reconstruct the temporal waveform by the inverse NFT (INFT) [28]. The temporal profile, optical spectrum, and eigenvalue distribution of filtered soliton are shown in Fig. 2. There is a reduction of the optical spectrum due to the taking-away of resonant CW background.

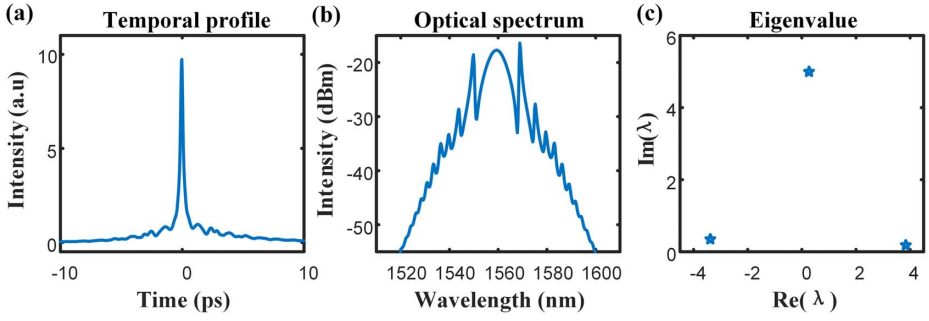

Fig. 1. (a) Temporal profile, (b) optical spectrum, and (c) eigenvalues of a pulse from the fiber laser.

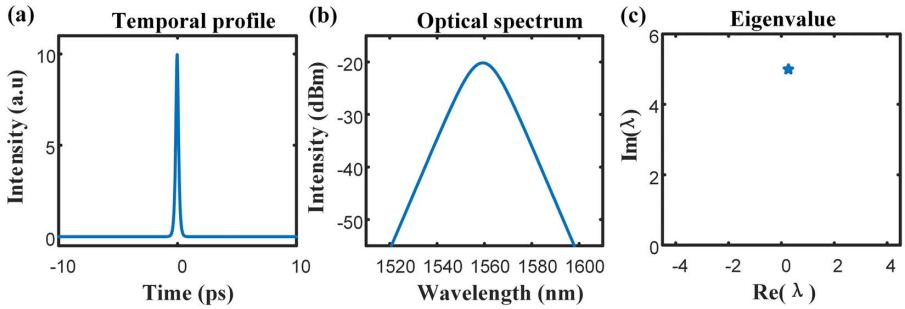

Fig. 2. (a) Temporal profile, (b) optical spectrum, and (c) eigenvalue of the filtered soliton.

Then, we analyze the starting dynamics of solitons in terms of the eigenvalue spectrum. Figure 3 shows the starting dynamics of the fiber laser. Starting from a small signal, the intensity evolution to a stable pulse is shown in Fig. 3(a), where different colors indicate different intensities. Figure 3(b) shows the evolution of eigenvalues versus round trips in 3D format, where the x axis is the real part, the y axis is the round trip, and the z axis is the imaginary part. During the soliton generation, there exist some eigenvalues with small imaginary parts in the nonlinear spectrum, corresponding to the resonant CW background. Then, the intensity evolution and eigenvalue evolution of the filtered soliton are shown in Figs. 3(c) and 3(d), respectively. After soliton distillation [28], we successfully obtained the soliton component of the generated pulse, i.e., the pure soliton.

When the pump power is increased to beyond a threshold, the pulse starts to periodically oscillate and return to itself every two round trips, which is called period doubling [29]. The dynamics of pulses in period doubling is shown in Fig. 4. The intensity of the pulse shuttles periodically between two states, as shown in Fig. 4(a). Figures 4(b) and 4(c) show the pulse temporal width and the imaginary part evolution of the eigenvalue, respectively. Synchronously, the pulse temporal width and eigenvalue oscillate with the same period of pulse intensity.

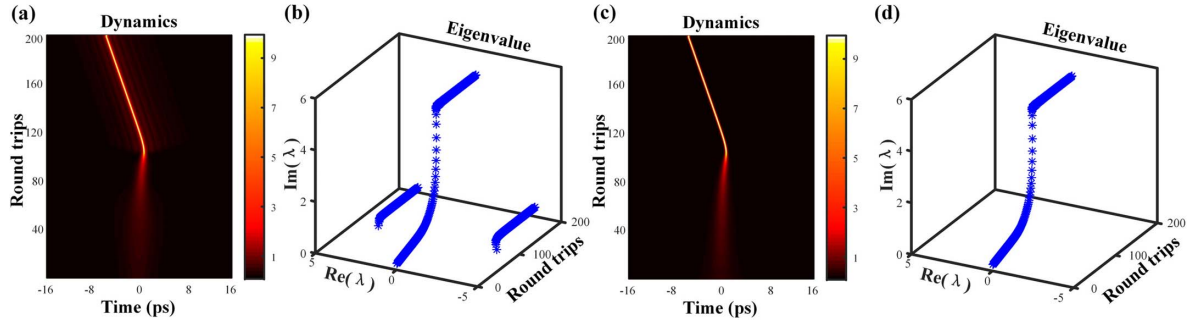

Fig. 3. NFT data evolution obtained from the measurement of the fiber laser: (a) real-time spatial–temporal dynamics of laser evolution from full-field measurements; (b) evolution of the eigenvalues; (c) dynamics of filtered soliton evolution; and (d) evolution of its eigenvalues.

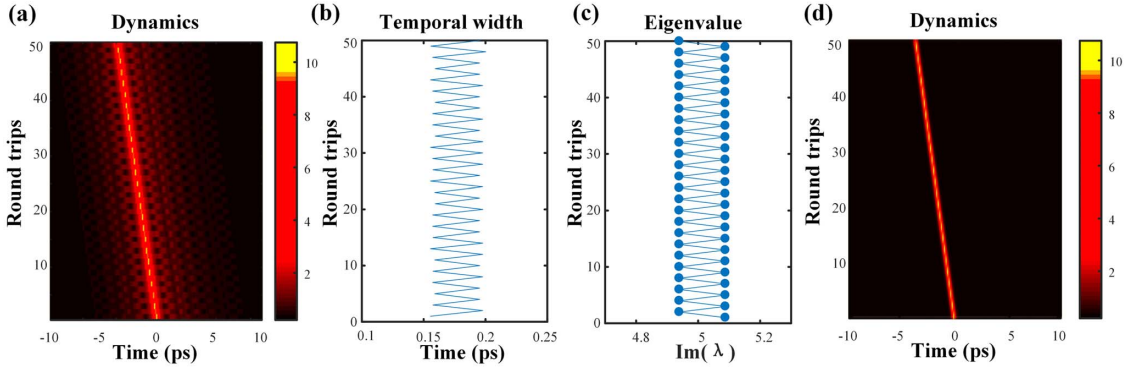

Fig. 4. NFT data evolution obtained from the output of the fiber laser in period doubling: (a) real-time spatial–temporal dynamics of laser evolution from full-field measurements; (b) the temporal width of the pulse during every round trip; (c) the evolution of the imaginary parts of eigenvalues; and (d) the evolution of filtered soliton evolution.

The intensity variation of the optical field is accompanied by a variation of eigenvalue spatial distribution. Such a relationship between the eigenvalue spectrum and the emergent features in the spatial–temporal dynamics demonstrates the effectiveness of the NFT formalism in revealing the underlying solitary modes embedded into the laser output. After soliton distillation, the intensity evolution of the filtered soliton is shown in Fig. 4(d). Distinctly from the stable pulse in Fig. 3, the pulses in period doubling have different eigenvalue distributions. This is because the imaginary part of the eigenvalue is related to the pulse intensity. Therefore, the change of eigenvalue imaginary part can reflect the periodic variation of pulse intensity as expected.

The temporal profiles and optical spectra of the two different states of pulses in period doubling are shown in Fig. 5. The pulse in state 1 has lower intensity and its temporal width is about 190 fs. Meanwhile, the pulse in state 2 has higher intensity and its temporal width is about 160 fs. After soliton distillation, the temporal profiles and optical spectra of the two different states of pure soliton are also shown in Fig. 5. The soliton in state 1 has relatively lower intensity and a narrower spectral bandwidth of ∼8 nm, while the soliton in state 2 has higher intensity and wider spectral bandwidth of ∼10 nm, which are qualitatively similar to the pulse.

Under appropriate parameter setting and operation conditions, typical emergence of multi-pulse states consisting of more than one pulse can be easily obtained from the fiber laser. Tightly bound solitons can be referred as soliton molecules if there exists strong soliton interaction [30]. Depending on the pulse separation and pulse intensity, the double pulse states can be classified into unstable and stable states, respectively. Setting the initial condition of the fiber laser as $q_0(t) = \mathrm{sech}(1.763t/3)$, the initial pulse can develop into unstable double pulses. The dynamic process of double pulses under unstable evolution can be obtained, as shown in Figs. 6(a)–6(d). The intensity evolution of the pulse is shown in Fig. 6(a), where different colors correspond to different intensities. During the evolution, the initial pulse splits into two pulses and their amplitudes sharply increase. After 60 round trips, the unstable double pulses are generated and there is an energy exchange between the two pulses, accompanied by the variation of their intensities. Figure 6(b) shows the imaginary part evolution of eigenvalues with respect to the round trip. Clearly, there are two eigenvalues, and each eigenvalue is associated with a pulse. Two eigenvalues first keep increasing and then increase and decrease alternately, revealing the energy exchange between the two pulses. After the soliton distillation, the temporal profiles of filtered soliton pairs are shown in Fig. 6(d). It is found that the soliton separation always reduced after the soliton distillation.

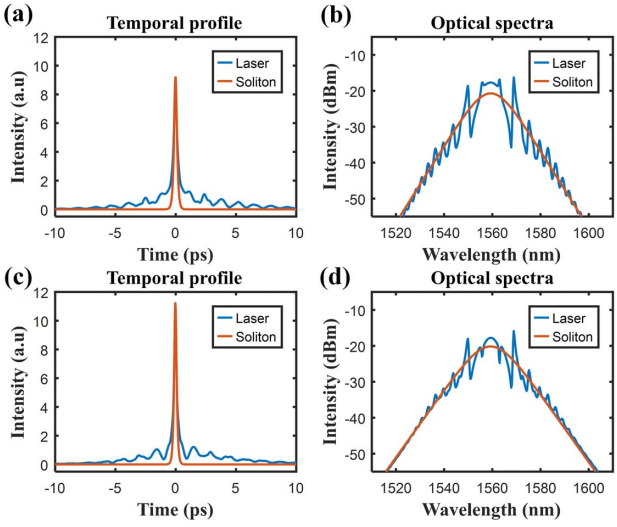

Fig. 5. Temporal profiles and optical spectra of the period doubling pulse without and with soliton distillation: (a), (b) state 1; (c), (d) state 2.

Changing the initial condition of the fiber laser as $q_0(t) = \mathrm{sech}[1.763(t + 6.5)/3] + \mathrm{sech}[1.763(t - 6.5)/3)]$, stable double pulses can be observed with appropriate parameter setting. Figure 6(e) shows the stable evolution of two pulses. However, it is difficult to distinguish whether there is energy exchange between the two pulses from Fig. 6(e) as their intensities are close to each other. During the evolution, there indeed exists a weak energy exchange between the two pulses, as shown in Fig. 6(f), when we monitored the stable evolution in terms of eigenvalues obtained from the NFT. The imaginary part evolution of eigenvalues with respect to the round trip clearly suggests the energy exchange. Therefore, the NFT method can disclose details during pulse evolution for the states of double pulses even when their pulse intensities are close.

Similar to the case of two unstable pulses, for the case of two stable pulses (identified by the pulse separation and pulse intensity), soliton separation reduces after distillation. Figures 6(g) and 6(h) show the temporal profiles of stable double pulses without and with soliton distillation, respectively. The intensity difference is shown in the zoom-in insets. It is verified that the CW background actually buffers solitons and affects the performance of the coexisting soliton pair.

We purposely changed the initial condition and achieved a state of two stable pulses with pulse separation of 26 ps, as shown in Figs. 6(i)–6(l). As the pulse separation is now much longer, the CW-based interaction between the two pulses should be weaker compared to the state shown in Figs. 6(e)–6(h), which is verified by the imaginary part evolution of eigenvalues as shown in Fig. 6(j). Now the imaginary part evolutions of eigenvalues of the two far-apart pulses are nearly overlapped entirely. Again, soliton separation reduces after distillation.

Adjusting the parameters in the laser cavity, the initial pulse $q_0(t) = \mathrm{sech}(1.763t/3)$ can also evolve into unstable triple pulses. Figures 7(a)–7(d) show the splitting dynamic process of the initial pulse $q_0(t)$. First, the initial pulse splits into two pulses, accompanied by the third pulse with relatively low amplitude, as shown in Fig. 7(a). Figure 7(b) shows the imaginary part evolution of eigenvalues with respect to the round trip. An eigenvalue with an imaginary part of ∼2 refers to the pulse with relatively low amplitude, around the first 50 round trips. Then, the unstable triple pulses are generated, and the eigenvalues increase and decrease alternately, revealing the energy exchange between the three pulses. Figures 7(c) and 7(d) show the temporal profiles of triple pulses with and without

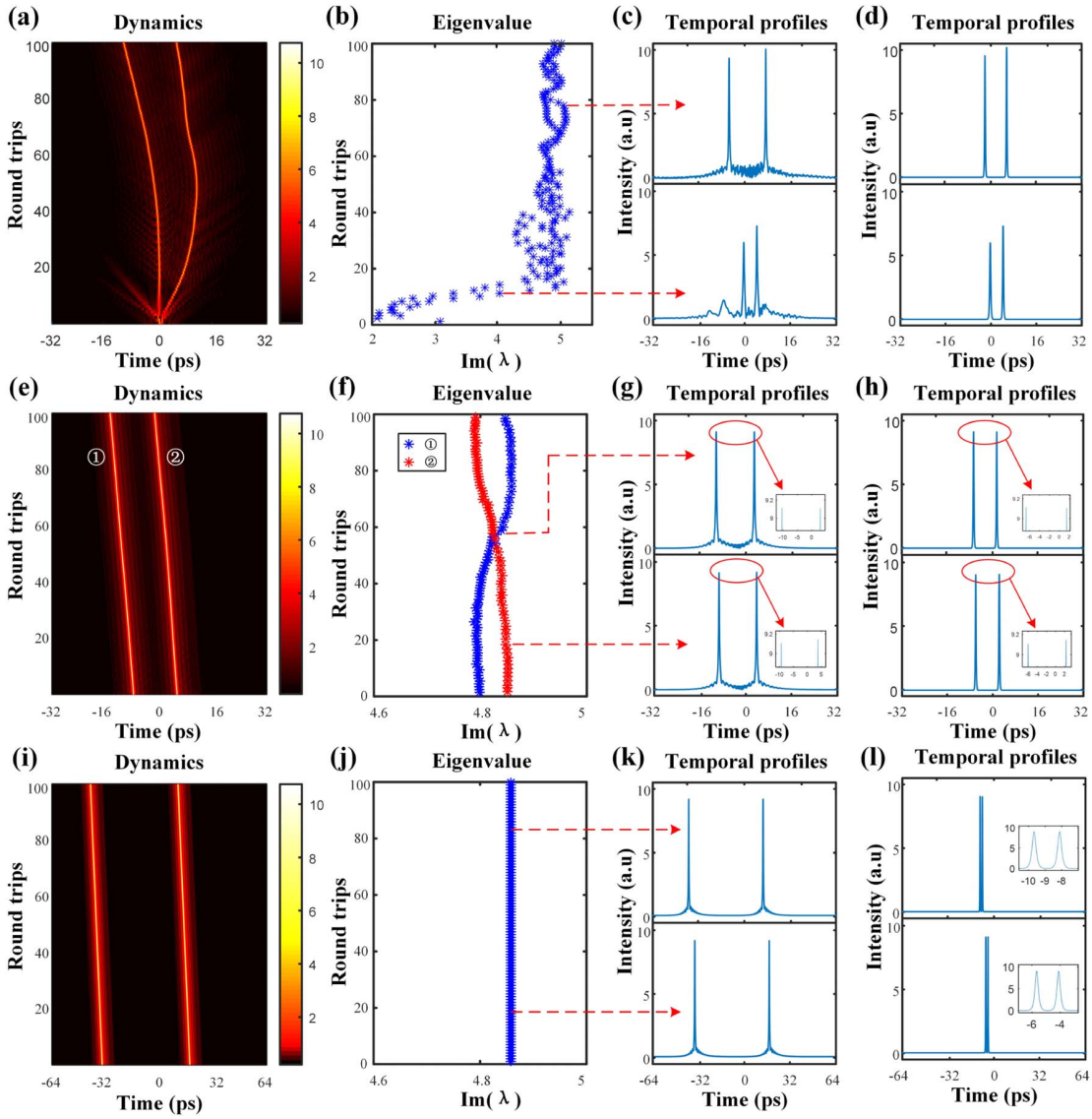

Fig. 6. NFT data evolution obtained from the double pulses under (a)–(d) unstable and (e)–(l) stable state: (a), (e), (i) real-time spatial–temporal dynamics of laser evolution from full-field measurements; (b), (f), (j) the evolution of the imaginary parts of eigenvalues; (c), (g), (k) the temporal profiles without soliton distillation; (d), (h), (l) the temporal profiles with soliton distillation.

soliton distillation, respectively. Similar to double pulses, the pulse separation of triple pulses reduces. Alternatively, setting the initial condition of the fiber laser as $q_0(t)=$ sech[1.763(t+T_0)/3]+sech(1.763t/3)+sech[1.763(t-T_0)/3], stable triple pulses can be easily obtained with appropriate parameter setting. Here T_0 is a variable, which is associated with pulse separation of the input pulse. When setting initial pulse separation $T_0 = 28$ ps, the dynamic process, eigenvalue evolution, temporal profiles, and filtered solitons of stable triple pulses are shown in Figs. 7(e)–7(h), respectively. Under stable operation, the pulse separation is relatively large. The inset in Fig. 7(f) shows the eigenvalues distributions of stable triple pulses. Their imaginary parts are approximately equal, revealing the triple-soliton pulses have approximately equal amplitudes in the time domain. Generally, the interaction between solitons is realized by the resonant and nonresonant CW background in the case of stable multi-pulses. As for stable triple pulses, in the nonlinear frequency domain, there are more eigenvalues with almost zero real parts on the bottom, due to the nonresonant CW background. After soliton distillation, soliton separation reduced significantly as both the resonant and nonresonant CW backgrounds are filtered out, as shown in Fig. 7(h).

Generally, triple pulses have three pulse separations and we name them ΔT_{12}, ΔT_{13}, and ΔT_{23}, respectively, as shown in Fig. 8(a). Figures 8(b) and 8(c) show the pulse separation and purified soliton separation with different initial pulse separation setting of T_0, respectively. Provided that $T_0 > 20$ ps, the pulse separation of the stable multiple pulse output from the fiber laser is always the same as the initial setting. When T_0 increases, the pulse separation accordingly increases. After soliton distillation, the soliton separation is greatly reduced. It is

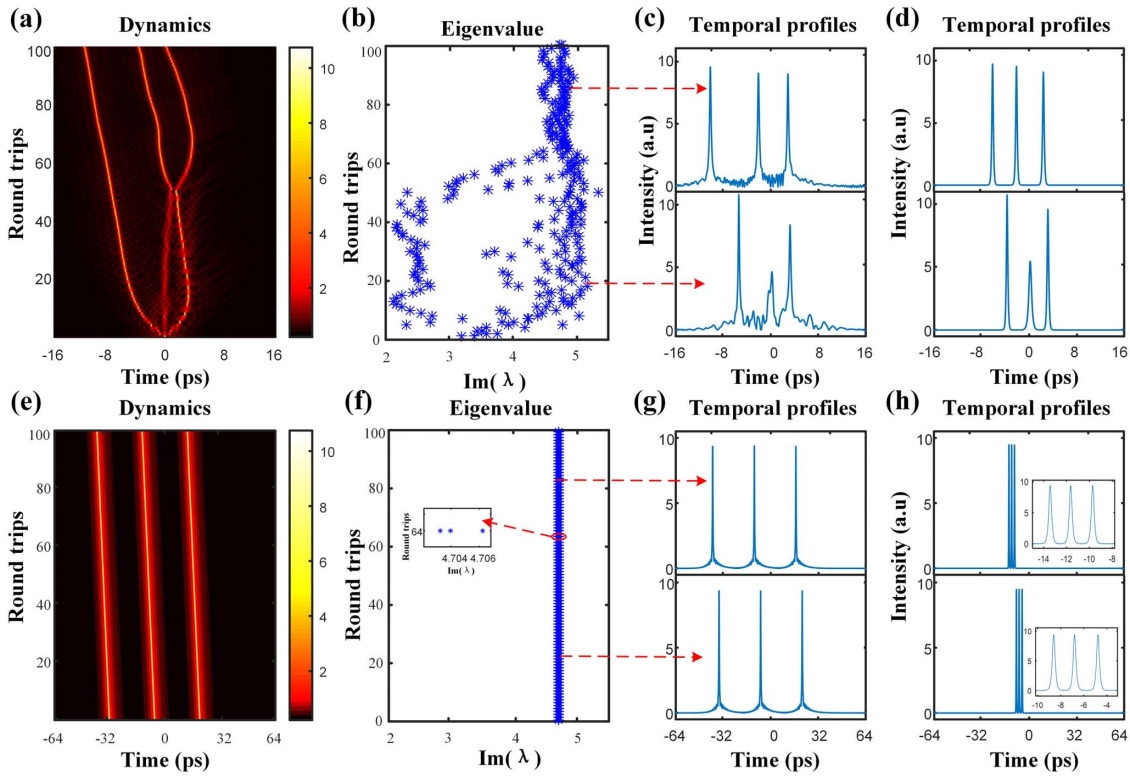

Fig. 7. NFT data evolution obtained from the triple pulses under (a)–(d) unstable and (e)–(h) stable state: (a), (e) real-time spatial–temporal dynamics of laser evolution from full-field measurements; (b), (f) the evolution of the imaginary parts of eigenvalues; (c), (g) the temporal profiles without soliton distillation; (d), (h) the temporal profiles with soliton distillation.

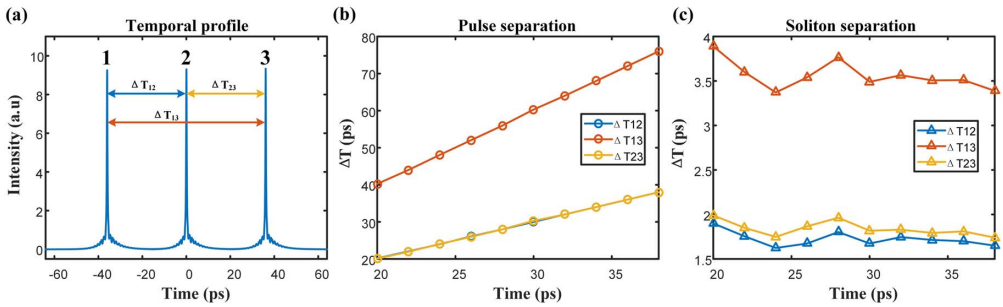

Fig. 8. (a) Three pulse separations of triple pulses, (b) pulse separation, and (c) filtered soliton separation with different initial pulse separation T_0.

straightforward that soliton separation can be manipulated and much reduced if the CW background is fully removed, which paves a way for manipulating solitons without CW background and shows a new viewpoint on acquisition of pure solitons from a fiber laser for soliton communication. It is feasible to obtain multiple solitons with much closer separation by employing the soliton distillation scheme.

3. CONCLUSION

In summary, the eigenvalues of a pulse can be obtained by using the NFT, whose real and imaginary parts correspond to the frequency and amplitude of the pulse, respectively. Pure solitons can be separated from the CW background according to different eigenvalue distributions. It is feasible to obtain NFT results from real-time spatial–temporal dynamics of various laser pulsing evolutions, for instance, single pulse, single pulse in period doubling, double pulses, and triple pulses. It is found that the imaginary part of the eigenvalue evolution of single pulse is consistent with its intensity evolution. As for coexisting multiple pulses, the imaginary parts of their eigenvalues alternatively increase or decrease during the evolution, revealing the changes in their intensity due to the energy exchange between the pulses during evolution. The degree of overlapping between the different evolutions of the imaginary parts of their eigenvalue of different pulses in the states of multiple pulses can be used to identify the pulse intensity difference, which is more obvious comparing with pulse intensity

evolutions. With the help of soliton distillation, we obtained pure solitons from those pulses. However, much closer soliton separation is always achieved. As a promising signal processing tool, the NFT paves a new way for investigating soliton interaction in nonlinear systems. Our results suggest that the NFT can be a featured characterization method in ultrafast optics. Recently, Vasylchenkova *et al.* have demonstrated a hardware implementation of the fast direct NFT operation [31], which makes the hardware realization of NFT possible in the future.

APPENDIX A

Generally, the NFT is a method to solve the initial value problem for the nonlinear evolution equation. In an optical fiber, where the signal evolution occurs along the fiber, the initial condition corresponds to the time-domain waveform at the transmitter and its evolution satisfies the NLSE. With the assumption of a noiseless and lossless fiber, the NLSE is a well-known and practically important example of the following integrable equation [20]:

$$j\frac{\partial q(t,z)}{\partial z}+\frac{1}{2}\cdot\frac{\partial^2 q(t,z)}{\partial t^2}+q(t,z)|q(t,z)|^2=0, \tag{A1}$$

where $q(t,z)$ is the evolution of a slow-varying optical field envelope. Similar to conventional Fourier transformation, initial conditions of the integrable nonlinear equation can be decomposed into nonlinear spectral data. As for the NLSE, this is realized through the solution of a linear scattering problem, known as the Zakharov–Shabat problem (ZSP) [32]. The NFT is calculated from specific solutions of the ZSP:

$$\frac{\mathrm{d}}{\mathrm{d}t}\begin{pmatrix}v_1(t,\lambda)\\ v_2(t,\lambda)\end{pmatrix}=\begin{pmatrix}-j\lambda & q(t)\\ -q^*(t) & j\lambda\end{pmatrix}\begin{pmatrix}v_1(t,\lambda)\\ v_2(t,\lambda)\end{pmatrix}, \tag{A2}$$

where $q(t)$ is the signal with vanishing boundary (in normalized units [20,26]) and λ is a spectral parameter, which plays a role of a nonlinear analog of frequency. $v_{1,2}$ are auxiliary functions and the scattering data $a(\lambda)$ and $b(\lambda)$ can be calculated from them:

$$a(\lambda)=\lim_{t\to\infty}v_1(t,\lambda)e^{j\lambda t},\ b(\lambda)=\lim_{t\to\infty}v_2(t,\lambda)e^{-j\lambda t}. \tag{A3}$$

Then the nonlinear spectrum of signal $q(t)$ is defined as

$$\tilde{q}_c(\lambda)=b(\lambda)/a(\lambda),\lambda\in R,\tilde{q}_d(\lambda)=b(\lambda_n)/a'(\lambda_n),\lambda_n\in C^+. \tag{A4}$$

$\tilde{q}_c(\lambda)$ is the continuous part of the nonlinear spectrum, which refers to the radiation component and converges to the ordinary Fourier spectrum at the low-power limit, and $\tilde{q}_d(\lambda)$ is the discrete part corresponding to the soliton component of the signal. λ_n is the eigenvalue in the upper half complex plane, which is defined as

$$a'(\lambda_n)=\left.\frac{\mathrm{d}a(\lambda)}{\mathrm{d}\lambda}\right|_{\lambda=\lambda_n}=0. \tag{A5}$$

As it is well known, the optical solitons are the balanced result of dispersion and nonlinearity, where they can propagate without distortion over the fiber. Similarly, for the pure NLSE, the complex eigenvalues also stay invariant during the pulse evolution. Therefore, by analyzing the nonlinear spectrum of the evolving signal, we can readily segregate the eigenvalue that refers to soliton components of the signal from the continuous spectrum. When calculating the nonlinear spectrum, different settings of normalization parameters may lead to different energy distributions between nonlinear spectral components [20]. Sugavanam *et al.* have shown that the NFT can yield an effective model of the laser radiation under z-independent or z-dependent field normalization conditions [26]. Since the nonlinear spectrum of a soliton only contains single discrete eigenvalue, its temporal waveform is expressed, after Ref. [33], in the following form:

$$q(t)=-2j\lambda_I e^{-j\angle\tilde{q}_d(\lambda_n)}\mathrm{sech}[2\lambda_I(t-t_0)]e^{-2j\lambda_R t},$$
$$t_0=\frac{1}{2\lambda_I}\ln\left[\frac{|\tilde{q}_d(\lambda_n)|}{2\lambda_I}\right], \tag{A6}$$

where λ_R and λ_I are the real and imaginary parts of eigenvalue λ_n, while the term $\angle\tilde{q}_d(\lambda_n)$ is the spectral phase, $|\tilde{q}_d(\lambda_n)|$ is the spectrum amplitude, and t_0 is the time center associated with λ_I and spectrum amplitude. As shown in Eq. (A6), the eigenvalue λ_n specifies the soliton parameters with an amplitude of $2\lambda_I$ and a frequency of $2\lambda_R$. Therefore, the nonlinear spectrum of multi-solitons has multi-eigenvalues and each eigenvalue corresponds to its own soliton component.

Figure 9 shows eigenvalues distribution of different solitons. We can clearly observe that, when the time center of the soliton changes, the eigenvalue still occurs at the same position, as shown in Fig. 9(b). There exist obvious isolated eigenvalues at $4j$ for soliton $q(t)=8\,\mathrm{sech}(8t)$, $4.5j$ for soliton $q(t)=9\,\mathrm{sech}(9t)$, and $5j$ for soliton $q(t)=10\,\mathrm{sech}(10t)$. Considering the physical meaning of the eigenvalue, a pulse with a form of $q(t)=A\,\mathrm{sech}(At)$ can be referred to a soliton containing a single nonlinear frequency $\frac{A}{2}j$. Figures 9(c) and 9(d) give the eigenvalue distribution of double solitons and triple solitons, respectively. Each soliton component has a single nonlinear frequency, and its nonlinear spectrum contains an isolated eigenvalue. Thus, the soliton can be precisely characterized by its discrete eigenvalue, which is the theoretical foundation of our research.

In our work, the NFT is used as a signal processing tool rather than to suppress the nonlinear transmission impairment arising in the nonlinear frequency-division multiplexing (NFDM) system [23–27]. Selecting appropriately normalized parameters is the key to analyze the laser radiation based on the NFT [26]. After traditional coherent detection, we applied the NFT methodology to obtain the eigenvalues of pulses from a passively mode-locked fiber laser. To achieve numerical analyzation without distortion, sufficient bandwidth and sampling rate of the coherent receiver are numerically set to avoid the pulse distortion.

A typical fiber laser mode locked by the nonlinear polarization rotation is chosen to generate ultrafast pulses [34], as shown in Fig. 10(a). An anomalous dispersion fiber cavity is achieved by using a section of 3 m long erbium-doped fiber with a dispersion parameter of 23 ps/(km·nm), in order to provide sufficient gain for the laser emission. The other fibers are standard SMFs, leading to a total cavity length of 6 m. A polarization controller is employed to adjust the polarization of the propagating light and a polarization-dependent isolator guarantees the unidirectional operation. The laser outputs are

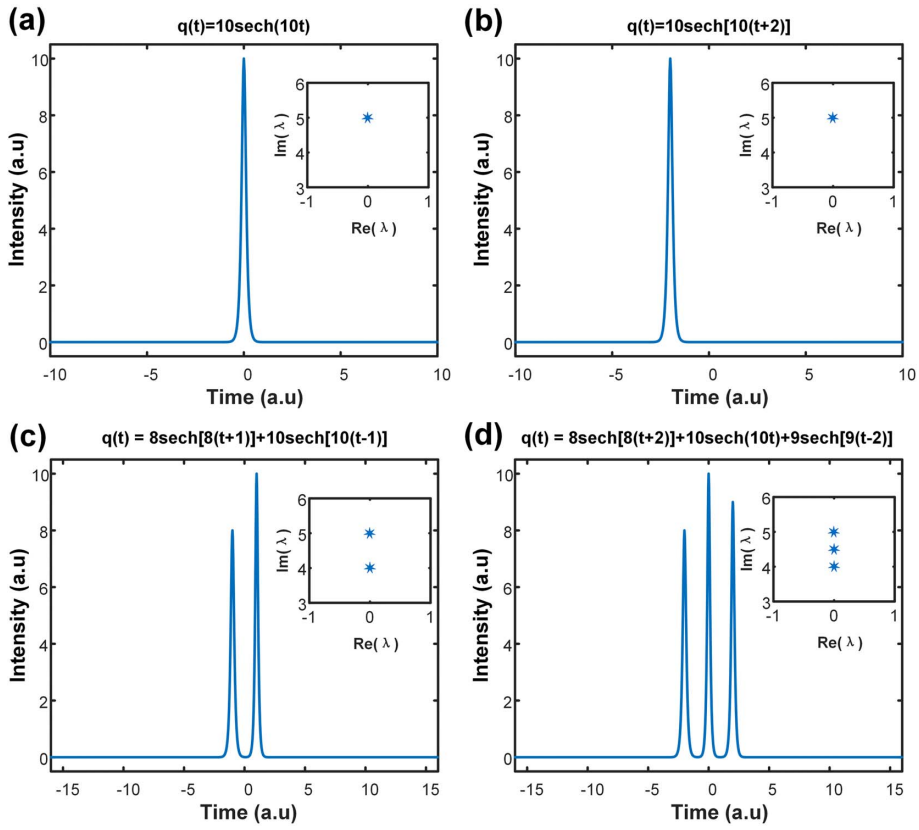

Fig. 9. Temporal profiles of (a) $q(t) = 10\,\mathrm{sech}(10t)$, (b) $q(t) = 10\,\mathrm{sech}[10(t + 2)]$, (c) $q(t) = 8\,\mathrm{sech}[8(t + 1)] + 10\,\mathrm{sech}[10(t - 1)]$, and (d) $q(t) = 8\,\mathrm{sech}[8(t + 2)] + 10\,\mathrm{sech}(10t) + 9\,\mathrm{sech}[9(t - 2)]$. Each inset shows the eigenvalue distribution of the corresponding temporal profile.

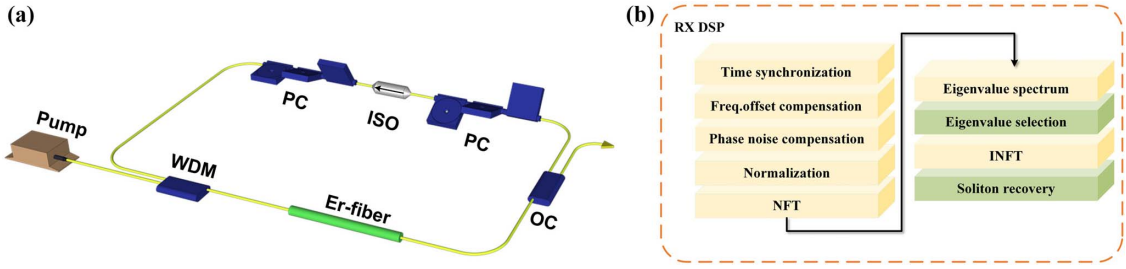

Fig. 10. (a) Passively mode-locked fiber laser. ISO, isolator; PC, polarization controller; WDM, wavelength-division multiplexer; OC, output coupler. (b) Corresponding digital signal processing (DSP) flows of coherent receiver.

hyperbolic secant pulses with a width of ~180 fs, center wavelength of 1560 nm, and spectral bandwidth of ~9 nm. The output ratio is 10%. During simulation, different kinds of pulse can be obtained by adjusting the pump power G and other parameter settings. For the ease of implementing traditional coherent detection, the output is mixed with a semiconductor laser source having a narrow linewidth of 100 kHz and acting as a local oscillator, with the help of 90° hybrid. Consequently, both in-phase (I) and the quadrature (Q) components can be secured. The optical-to-electrical conversion is realized by a pair of balanced photodetectors and two electrical outputs are digitalized by a high-speed oscilloscope. Figure 10(b) shows the corresponding digital signal process flows of coherent detection. Here, both frequency offset and phase noise effects can be mitigated the same as that for the NFDM transmission [35,36].

Then, the NFT determined eigenvalue can be calculated from the full-field information of the pulse. An important step for obtaining the nonlinear frequency spectrum is the normalization of the input field, scaling the time and amplitude [20,26]. Here, we normalize time to a scale $T_s = 1$ ps, which approximately contains 99% of the signal energy averaged over many round trips. The amplitude is also normalized with a scale Q_s, which is the squared root of the power of a hyperbolic secant signal with a time-width equal to a time window containing 99% of the signal energy. Finally, after filtering out the

eigenvalues of the resonant CW background, the pure solitons can be reconstructed by INFT. In practice, for the ease of experimental verification, a fiber laser with output pulse duration that can be covered by the PD bandwidth should be specially designed and exploited.

Funding. National Key R&D Program of China (2018YFB1801001); Fundamental Research Funds for the Central Universities (HUST 2020kfyXJJS007); National Natural Science Foundation of China (61875061); Protocol of the 9th Session of China-Croatia Scientific and Technological Cooperation Committee (9-28); Protocol of the 38th Session of China-Poland Scientific and Technological Cooperation Committee (6); National Agency for Academic Exchange in Poland (PPN/BCN/2019/1/00068); Foundation for Polish Science First TEAM POIR (04.04.00-00-1D64/16).

Disclosures. The authors declare no conflicts of interest.

Data Availability. Data underlying the results presented in this paper are not publicly available at this time but may be obtained from the authors upon reasonable request.

REFERENCES

1. P. M. W. French, "The generation of ultrashort pulses," Rep. Prog. Phys. **58**, 169–267 (1995).
2. U. Keller, "Recent developments in compact ultrafast lasers," Nature **424**, 831–838 (2003).
3. A. Martinez and Z. P. Sun, "Nanotube and graphene saturable absorbers for fiber lasers," Nat. Photonics **7**, 842–845 (2013).
4. U. Andral, R. S. Fodil, F. Amrani, F. Billard, E. Hertz, and P. Grelu, "Fiber laser mode locked through an evolutionary algorithm," Optica **2**, 275–278 (2015).
5. S. Kobtsev, S. Kukarin, S. Smirnov, S. K. Turitsyn, and A. Latkin, "Generation of double-scale femto/pico-second optical lumps in mode-locked fiber lasers," Opt. Express **17**, 20707–20713 (2009).
6. N. Tarasov, A. M. Perego, D. V. Churkin, K. Staliunas, and S. K. Turitsyn, "Mode-locking via dissipative Faraday instability," Nat. Commun. **7**, 12441 (2016).
7. J. Xu, L. Huang, M. Jiang, J. Ye, P. Ma, J. Leng, J. Wu, H. Zhang, and P. Zhou, "Near-diffraction-limited linearly polarized narrow-linewidth random fiber laser with record kilowatt output," Photon. Res. **5**, 350–354 (2017).
8. A. Chong, J. Buckley, W. Renninger, and F. Wise, "All-normal-dispersion femtosecond fiber laser," Opt. Express **14**, 10095–10100 (2006).
9. A. F. J. Runge, N. G. R. Broderick, and M. Erkintalo, "Observation of soliton explosions in a passively mode-locked fiber laser," Optica **2**, 36–39 (2015).
10. G. Herink, F. Kurtz, B. Jalali, D. R. Solli, and C. Ropers, "Real-time spectral interferometry probes the internal dynamics of femtosecond soliton molecules," Science **356**, 50–54 (2017).
11. K. Krupa, K. Nithyanandan, and G. Grelu, "Vector dynamics of incoherent dissipative optical solitons," Optica **4**, 1239–1244 (2017).
12. X. Liu, D. Popa, and N. Akhmediev, "Revealing the transition dynamics from *Q* switching to mode locking in a soliton laser," Phys. Rev. Lett. **123**, 093901 (2019).
13. X. Liu and M. Pang, "Revealing the buildup dynamics of harmonic mode-locking states in ultrafast lasers," Laser Photonics Rev. **13**, 1800333 (2019).
14. P. Suret, R. E. Koussaifi, A. Tikan, C. Evain, S. Randoux, C. Szwaj, and S. Bielawski, "Direct observation of rogue waves in optical turbulence using time microscopy," Nat. Commun. **7**, 13136 (2016).
15. A. Tikan, C. Billet, G. El, A. Tovbis, M. Bertola, T. Sylvestre, F. Gustave, S. Randoux, G. Genty, P. Suret, and J. M. Dudley, "Universality of the peregrine soliton in the focusing dynamics of the cubic nonlinear Schrödinger equation," Phys. Rev. Lett. **119**, 033901 (2017).
16. S. M. J. Kelly, "Characteristic sideband instability of periodically amplified average soliton," Electron. Lett. **28**, 806–807 (1992).
17. M. Liu, H. J. Chen, A. P. Luo, G. Y. Zhou, and Z. C. Luo, "Identification of coherent and incoherent spectral sidebands in an ultrafast fiber laser," IEEE J. Sel. Top. Quantum Electron. **24**, 1100606 (2018).
18. A. Komarov, K. Komarov, A. Niang, and F. Sanchez, "Nature of soliton interaction in fiber lasers with continuous external optical injection," Phys. Rev. A **89**, 013833 (2014).
19. S. K. Turitsyn, J. E. Prilepsky, S. T. Le, S. Wahls, L. L. Frumin, M. Kamalian, and S. A. Derevyanko, "Nonlinear Fourier transform for optical data processing and transmission: advances and perspectives," Optica **4**, 307–322 (2017).
20. M. I. Yousefi and F. R. Kschischang, "Information transmission using the nonlinear Fourier transform. Part II: numerical methods," IEEE Trans. Inf. Theory **60**, 4329–4345 (2014).
21. J. E. Prilepsky, S. A. Derevyanko, K. J. Blow, I. Gabitov, and S. K. Turitsyn, "Nonlinear inverse synthesis and eigenvalue division multiplexing in optical fiber channels," Phys. Rev. Lett. **113**, 013901 (2014).
22. S. T. Le, V. Aref, and H. Buelow, "Nonlinear signal multiplexing for communication beyond the Kerr nonlinearity limit," Nat. Photonics **11**, 570–576 (2017).
23. S. Randoux, P. Suret, and G. El, "Inverse scattering transform analysis of rogue waves using local periodization procedure," Sci. Rep. **6**, 29238 (2016).
24. J. Wang, A. Sheng, X. Huang, R. Li, and G. He, "Eigenvalue spectrum analysis for temporal signals of Kerr optical frequency combs based on nonlinear Fourier transform," Chin. Phys. B **29**, 034207 (2020).
25. P. Ryczkowski, M. Närhi, C. Billet, J.-M. Merolla, G. Genty, and J. M. Dudley, "Real-time full-field characterization of transient dissipative soliton dynamics in a mode-locked laser," Nat. Photonics **12**, 221–227 (2018).
26. S. Sugavanam, M. K. Kopae, J. Peng, J. E. Prilepsky, and S. K. Turitsyn, "Analysis of laser radiation using the nonlinear Fourier transform," Nat. Commun. **10**, 5663 (2019).
27. I. S. Chekhovskoy, O. V. Shtyrina, M. P. Fedoruk, S. B. Medvedev, and S. K. Turitsyn, "Nonlinear Fourier transform for analysis of coherent structures in dissipative systems," Phys. Rev. Lett. **122**, 153901 (2019).
28. Y. Wang, S. Fu, C. Zhang, X. Tang, J. Kong, J. H. Lee, and L. M. Zhao, "Soliton distillation of pulses from a fiber laser," J. Lightwave Technol. **39**, 2542–2546 (2021).
29. L. M. Zhao, D. Y. Tang, F. Lin, and B. Zhao, "Observation of period-doubling bifurcations in a femtosecond fiber soliton laser with dispersion management cavity," Opt. Express **12**, 4573–4578 (2004).
30. L. Li, H. Huang, L. Su, D. Y. Shen, D. Y. Tang, M. Klimczak, and L. M. Zhao, "Various soliton molecules in fiber systems," Appl. Opt. **58**, 2745–2753 (2019).
31. A. Vasylchenkova, D. Salnikov, D. Karaman, O. G. Vasylchenkov, and J. E. Prilepskiy, "Fixed-point realisation of fast nonlinear Fourier transform algorithm for FPGA implementation of optical data processing," Proc. SPIE **11770**, 1177016 (2021).
32. V. E. Zakharov and A. B. Shabat, "Exact theory of two-dimensional self-focusing and one-dimensional self-modulation of waves in nonlinear media," J. Exp. Theor. Phys. **34**, 62–69 (1972).
33. T. Gui, C. Lu, A. P. L. Lau, and P. K. A. Wai, "High-order modulation on a single discrete eigenvalue for optical communications based on nonlinear Fourier transform," Opt. Express **25**, 20286–20297 (2017).
34. L. M. Zhao, D. Y. Tang, H. Y. Tam, and C. Lu, "Pulse breaking recovery in fiber lasers," Opt. Express **16**, 12102–12107 (2008).
35. Z. Zheng, X. Zhang, R. Yu, L. Xi, and X. Zhang, "Frequency offset estimation for nonlinear frequency division multiplexing with discrete spectrum modulation," Opt. Express **27**, 28223–28238 (2019).
36. Y. Wang, R. Xin, S. Fu, M. Tang, and D. Liu, "Laser linewidth tolerance for nonlinear frequency division multiplexing transmission with discrete spectrum modulation," Opt. Express **28**, 9642–9652 (2020).